

# Observation of hydrodynamic-like behavior in 3D Dirac semimetal

## ZrTe<sub>5</sub>

Chang-woo Cho<sup>1,2</sup>, Peipei Wang<sup>1</sup>, Fangdong Tang<sup>1</sup>, Sungkyun Park<sup>2</sup>, Mingquan He<sup>3</sup>, Rolf Lortz<sup>4</sup>, Genda Gu<sup>5</sup>, and Liyuan Zhang<sup>1,+</sup>

<sup>1</sup>*Department of Physics, Southern University of Science and Technology, 1088 Xueyuan Road, Nanshan District, Shenzhen, Guangdong 518055, China*

<sup>2</sup>*Department of Physics, Pusan National University, Busan 46241, South Korea*

<sup>3</sup>*Chongqing Key Laboratory of Soft Condensed Matter Physics and Smart Materials, College of Physics, Chongqing University, Chongqing 401331, China*

<sup>4</sup>*Department of Physics, The Hong Kong University of Science and Technology, Clear Water Bay, Kowloon, Hong Kong*

<sup>5</sup>*Condensed Matter Physics and Materials Science Department, Brookhaven National Laboratory, Upton, NY 11973, USA*

The phonon hydrodynamic system has only been detected experimentally in the limited compounds because of its stringent condition to appear. Herein, we elucidate the existence of hydrodynamic features driven by the collective excitation of Dirac fluid in semimetal ZrTe<sub>5</sub>. By measuring the electrical and the thermal property in a wide temperature range, we find the regime as satisfying phonon hydrodynamic-like characteristics with two representative experimental evidence: faster evolution of thermal conductivity than the ballistic regime and the existence of a local maximum of effective mean-free-path. Unlike the phononic hydrodynamics, a magnitude of hundreds violated Wiedemann-Franz law, and phonon-dragged anomalies can be seen, which provide us as a signature of the Dirac fluid in this system.

---

<sup>+</sup> corresponding author: zhangly@sustech.edu.cn

## Introduction

Phonon-dominant heat conduction is described by Fourier's law at which phonons are scattered by other phonons, impurities, and boundaries<sup>1-3</sup>. Such events occur through the momentum-relaxing process, so-called Umklapp scattering (hereafter U-scattering). During this process, heat currents are degraded, and the crystal momentum does not conserve<sup>1-3</sup>. On the other hand, Fourier's law is no longer valid when the temperature is sufficiently low in which the crystal momentum is preserved due to dominant Normal-scattering (hereafter N-scattering)<sup>4-6</sup>. These two types of scattering mechanisms are known for a diffusive and a ballistic regime, respectively, have been confirmed in many materials for over 50 years<sup>4-6</sup>.

Meanwhile, the unusual transport phenomena between the ballistic and the diffusive regimes have reported on low-dimensional materials recently<sup>7-12</sup>, in which thermal conductivity  $\kappa$  evolves faster than the one in the ballistic range<sup>8, 12</sup>. Such an intermediate domain is named the hydrodynamic because it is analog with macroscopic transport phenomena in water fluids<sup>13, 14</sup>. If limited to the phononic hydrodynamic system, two characteristic features are seen: the Poiseuille flow and the second-sound<sup>14-16</sup>. The former is described by the steady-state phonon flow, at which thermal resistance is diffuse due to the boundary scattering combined with N-scattering. The latter is the wave-propagation of a temperature gradient without significant damping. The phonon Poiseuille flow could be confirmed through the temperature, and the sample width dependencies of  $\kappa$ <sup>8, 9, 12</sup>.

Despite the fascination of hydrodynamics, it is only observed in a narrow temperature range and required remarkably low-temperature with abundant N-scattering as well as an appropriate sample size. The reported temperature range for phonon Poiseuille flow is 0.5 – 1.0 K in a suspended graphene<sup>7, 16</sup>. It is because U-scattering overwhelms N-scattering in almost any temperature range, excluding the significantly low temperatures. However, the phonons are not the primary heat carriers when the N-scattering dominates. Instead the electrons are mainly contributing to the scattering process in general. For these reasons, hydrodynamic-like behavior has been detected experimentally in less than a handful of compounds, such as black P<sup>9</sup>, SrTiO<sub>3</sub><sup>17</sup>, and thin-graphite<sup>8</sup>. Therefore, finding a new material that observable the hydrodynamics contributed by the phonons or other excitations is of significant interest in the condensed matter society.

In this letter, we investigate the thermal and electrical transport property for ZrTe<sub>5</sub> single crystals to explore the hydrodynamic property. Indeed, the ZrTe<sub>5</sub> study is initiated decades ago due to its sizable thermoelectric performance and the resistivity anomaly. It is renewed attraction recently due to non-trivial topological phenomena such as 3D quantum Hall effect<sup>18</sup>, quantum spin Hall effect on a monolayer<sup>19</sup>, and chiral magnetic effect<sup>20</sup>, etc. Furthermore, it

reported that bulk  $\text{ZrTe}_5$  is sitting on the boundary between weak- and strong-topological insulator so that an external perturbation easily influences its topology<sup>21-23</sup>. Herein, we may add the list of abnormal phenomena in this composition as a hydrodynamic in Dirac-fluid (DF), which is unexpected. We present two experimental signatures for phonon hydrodynamic-like phenomena with the transport measurements as a faster evolution of  $\kappa$  rather than the ballistic regime and a local maximum of effective mean-free-path (MFP). As a result, our thermal Hall experimental results seem to support the DF scenario, unlike the conventional phononic hydrodynamics. We hope that these observations have significant consequences for the ongoing research in finding the different types of quasiparticles hydrodynamics and provide a deeper understanding of it.

## Experiment

Ultrahigh quality of single crystals of  $\text{ZrTe}_5$  were grown by the tellurium flux method. Thanks to the relatively large size of needle-like single crystals ( $l \times w \times t$ , sample #1:  $3.20 \times 0.30 \times 0.08 \text{ mm}^3$ , sample #2:  $2.90 \times 0.30 \times 0.21 \text{ mm}^3$ ), we performed the electrical and thermal transport experiments on the same bulk sample. Details of sample growth and structural properties can be found elsewhere<sup>18,20,24</sup>. In the main text, we defined the longest (shortest) dimension is along the  $a$ -axis ( $b$ -axis, corresponding to the stacking layers direction).

For the electrical transport measurement, we carried it out with the standard Hall-bar method applying an alternative current of 0.01-0.1 mA amplitude and a frequency of 10-20 Hz. The magnetic field was applied to the perpendicular direction with respect to the  $ac$ -plane.

To measure thermal transport such a needle-like shape of  $\text{ZrTe}_5$ , we used well-known steady-state one-heater and three-thermometers method. One end of a  $\sim 4.0 \text{ mm}$  long needle-like sample attached to a cooper heat sink, while a small  $\sim 100 \text{ Ohms}$  resistor and three well-calibrated Cernox thermometers were connected through the Ag (100  $\mu\text{m}$ ) and Pt/W wires (25  $\mu\text{m}$ ), respectively (see supplementary **Fig. S1**). With help of three lock-in amplifiers and three thermometer chips, we successfully obtained the longitudinal and the transverse thermal gradient simultaneously. In order to eliminate spurious longitudinal (or transverse) components, we measured the magneto-thermal conductivity at the opposite field directions and averaged by subtracting (or summation) each directional data. Since the sensitivity of thermometers used in this experiment becomes insensitive into higher temperatures, we changed to thermocouple method to record the thermal gradient at a high temperature regime (above  $\sim 20 \text{ K}$ ). In the overlapped range (about 10-20 K), we confirmed the well-matched  $\kappa$  within error bar, an example for sample #2 is presented in supplementary **Fig. S2**.

## Results and Discussion

Since our primary interest is the hydrodynamic-like system, it is essential to check whether the samples used in this study are clean enough. Otherwise, it is hardly observable due to the lacking of N-scattering even in the low temperatures. **Figure 1a** presents the electrical resistivity in a temperature range of 0.3 to 300 K at a zero magnetic field. A characteristic peak around  $\sim 90$  K ( $T_p$ ) revealed on both samples (sample #1: 84 K and sample #2: 89 K), which is well-known that the  $\text{ZrTe}_5$  electronic system transforms from a “hole” insulator at high  $T$  to an “electron” metal at low  $T$ <sup>25</sup>. In **Fig. 1b** and **c**, we depict the temperature-dependent dominant carrier density  $n$  and the mobility  $\mu$ , respectively. Both quantities are extracted from a two-band model fit ( $T > 40$  K) and the linear fit near the zero-field data taken by the Hall measurement ( $T < 40$  K). It exhibits an evident sign change of  $n$  with the exceptionally low density ( $\sim 10^{16}$  to  $\sim 10^{17}$   $\text{cm}^{-3}$ ) and the gradual increment of  $\mu$  with ultrahigh values ( $\sim 10^4$  to  $\sim 10^5$   $\text{cm}^2\text{V}^{-1}\text{s}^{-1}$ ) at low  $T$ . All the values are comparable with our previous observation,<sup>18</sup> thus it guarantees the excellent crystalline quality of samples and enables us the examination of a hydrodynamic-like regime as follow.

Let us explore the experimental evidence for hydrodynamics in our  $\text{ZrTe}_5$  from now on. The first clue is to find the faster evolution of  $\kappa$  rather than  $T^3$ . To test it, we plot the temperature dependence of the total thermal conductivity  $\kappa_{tot}$  (open squares in sample #1 and circles in sample #2), and the electronic thermal conductivity  $\kappa_e$  (solid lines) in **Fig. 2**. Note that the only  $\kappa_{tot}$  is the measured value,  $\kappa_e$  is obtained from the Wiedemann-Franz (WF) law ( $\kappa_e = \frac{T}{\rho} L_0$ , Lorenz number  $L_0 = 2.44 \times 10^{-8} \text{ W}\Omega\text{K}^{-2}$ ). For better clarity, it is plotted on a log-log scale here. In a high  $T$  regime (between about 30 K to 300 K), it is governed by the perfect  $1/T$  dependence regardless of samples (see supplementary **Fig. S2**), which implies that the U-scattering is the most prominent process in this range. After passing through the  $\kappa_{tot}$  maxima, it begins to decrease, indicating the N-scattering process stands out. For sample #2, while the evolution of  $\kappa_{tot}$  is ambiguous if this is faster than  $T^3$  behavior until  $\sim 5$  K, it is rapidly decreasing when the temperature down to  $\sim 2$  K where the slope of  $\kappa_{tot}$  is steeper than  $T^5$  dependence (dashed line in **Fig. 2**). The result of sample #1 shows in a similar way with a little slower temperature processing. It should mention that  $\kappa_e$  shows an irregular behavior in the sufficiently low  $T$ , where it must get close to  $\kappa_{tot}$  because the thermal energy in low  $T$  is mainly transferred by the charged carriers. However, we do not see any convergence in the practical temperature limit (0.3 to 300 K). Below 1 K,  $\kappa_e$  is still smaller than  $\kappa_{tot}$  by a factor of hundreds. We will discuss more details later on with the large-violation of WF-law.

In the vicinity of the hydrodynamic-like regime, we additionally observe the anomalies. In **Fig. 3a** and **b**, we present the enlarged electrical resistivity  $\rho$  and  $\kappa_{tot}$  versus  $T$  curves for sample

#2. At a glance, the  $\rho$  exhibits a typical  $T$ -quadratic Fermi-liquid ( $FL$ ) behavior in a variety of 6-30 K. Upon cooling further, the  $\rho$  begins to deviate from the  $\sim 6$  K ( $T_a$ ), and more or less linearly drop down without saturation or reaches the complete zero resistance like superconductivity within our experimental limit. A power-law scaling (i.e.,  $\rho = \rho_0 + AT^2$ ) between 6 to 30 K yields a residual resistivity  $\rho_0 \approx 0.154$  m $\Omega$  cm and the pre-factor  $A \approx 0.098$  m $\Omega$  cm  $K^{-2}$ . In the  $\kappa_{tot}$  versus  $T$  result (**Fig. 3b**), it is showing a step-like anomaly which perfectly coincides with  $T_a$ . The origin of the breakdown of  $FL$  as well as a  $\kappa$  anomaly was thought to be arising from a superconducting transition at the initial stage. However, we rule this possibility out based on the pressure-induced superconductivity study in Ref<sup>26</sup>. According to their results, when pressure applied to 6.7 GPa, superconductivity begins to appear at  $T_c \sim 1.8$  K with an acute phase transition<sup>26</sup>. Moreover, the estimation of the upper critical field was about 1.5 T at 14.6 GPa<sup>26</sup>. These findings are inconsistent with current observations that in-plane resistivity reduction does not occur as sharply as the superconducting transition. Also it seems quite robust to the external magnetic fields (see supplementary **Fig. S3**). One interesting is that non- $FL$  behavior seen only to sample #2. It is assuming that this might be due to the initial growth environment difference. ZrTe<sub>5</sub> is a highly sensitive material to growth conditions, resulting in its electronic and thermal properties. Another possibility is that the base temperature was not cool enough to be seen  $FL$  in sample #1.

On the other hand, a common anomaly for our samples is found in  $T$ -dependent  $\kappa/T^3$  and Lorenz ratio ( $L/L_0$ ), as shown in **Fig. 3c** and **d**. These anomalies are taking place on the onset points of a hydrodynamic-like regime. It is reasonable to say such a peaky anomaly originated from the phonon-drag effect because no signs are seen in the  $\rho$  vs  $T$  result (see **Fig. 2**), which means phonons rather than the electrical contribution attributes this anomaly. In Ref<sup>27</sup>, a pronounced phonon-drag peak in the low  $T$  thermopower was also reported in Dirac semimetal PtSn<sub>4</sub> where the peak observed solely thermal transport results similar to the present results.

Next, we return our interest to the effective quasiparticle MFP, another critical sign of phonon hydrodynamics. In most previous studies, the magnitude of MFP has been estimated through the simple relation  $\kappa_{ph} = \frac{1}{3}C_{ph}v_sl_{ph}$ , where  $C_{ph}$ ,  $v_s$ , and  $l_{ph}$  denote the phonon specific heat, sound velocity, and phonon MFP, respectively. Instead of a conventional way, we try to measure the thermal Hall effect since it could be a direct probe to examine the quasiparticle dynamics but has rarely performed to topological materials to date because of its difficulty to obtain the high-quality data.

**Figure 4a** shows the field dependence of the thermal Hall resistivity  $\omega_{xy}$  ( $= \frac{wt}{l} \left( \frac{\Delta T_{xy}}{P} \right)$ , where  $\Delta T_{xy}$  and  $P$  denote the temperature gradient between two points along the transverse direction and the heat power, respectively) in a narrow range of -1.0 to 1.0 T. In the main text, we only

plot in case of sample #1. The value of  $\omega_{xy}$  is nearly zero independent of measured temperatures. However, in a weak field range ( $|B| < \sim 0.1$  T), an asymmetrical thermal Hall feature is found, and it becomes more severe as decreasing  $T$ .

In order to evaluate of heat deviation degree, we further plot the thermal Hall angle  $\tan \theta_H$  ( $= \frac{\kappa_{xy}}{\kappa_{xx}}$ ) as a function of  $B$ -fields with various temperatures, which is presented in **Fig. 4b**.

Remarkably, these show a qualitatively identical tendency, which indicate a substantial deviation of thermal gradient between the longitudinal and the transverse directions upon applying  $B$ -fields, however it abruptly suppressed and eventually disappeared.

In **Fig. 4c**, we reveal the zero-field limit ( $B \rightarrow 0$ ) of  $\tan \theta_H / B$  (hereafter  $[\tan \theta_H / B]_0$ ), which is usually proportional to the effective MFP of quasiparticles<sup>28</sup>. A striking feature of  $[\tan \theta_H / B]_0$  is an existence of the local peak (marked with vertical arrows) corresponding temperatures at  $\sim 2$  K (sample #1) and  $\sim 6$  K (sample #2), which are exactly matched with the onset of hydrodynamic-like regime we have seen. It is worthwhile to mention that the thermal Hall signal originates from the electronic contribution in principle since the neutrally charged quasiparticles are not affected by a magnetic field. Magnons can be an exceptional case. However, it could not be our consideration because the magnon behavior should be more distinct as increasing  $B$ -field, which contradicts our observation.

So far, we have shown the hydrodynamic-like features with the electrical and the thermal transport results. The following question is what kinds of quasiparticle excitations or their interactions caused the hydrodynamics to realize. First of all, we may extract the electron-electron hydrodynamic scenario. According to zero-field limit electronic Hall angle result ( $[\tan \theta_e / B]_0$ , see inset of **Fig. 4c**), it is continuously increasing when  $T$  goes down until  $\sim 10$  K and then saturated in a low  $T$  regime. This means the electron-electron scattering process is not virtually affected by the whole scattering system below 10 K.

The next option is electron-phonon fluid, in which the electron-phonon scattering process is the fastest so that their momentum can be quasi-conserved. Previously studied electron-phonon cases, their results came out somehow similar to ours. For instance, we find the phonon-drag effect in thermal transport and the breakdown of WF law, which are suggested in Ref<sup>27</sup> as evidence of electron-phonon fluid. A difference with the present study is that the magnitude of  $L/L_0$ . While  $L/L_0$  in our  $\text{ZrTe}_5$  deviates from the value of 1 in an entire temperatures range and have a large value over hundreds (see **Fig. 3d**), the data presented in  $\text{PtSn}_4$  showed opposite results ( $L/L_0 < 1$ ) at a hydrodynamic regime, as they argued this is an indication of a significant inelastic electron-phonon scattering<sup>11</sup>. In this regard, we also exclude electron-phonon induced hydrodynamics.

The DF scenario is our last choice in this letter. This kind of strange metal was introduced by Crossno et al in 2005 to describe the hydrodynamic behavior at the charge neutrality point<sup>11</sup>.

As noted above, used  $\text{ZrTe}_5$  single crystals exhibit ultra-high mobility due to the extraordinary high-purity, and their bipolar carrier types are more or less compensated at low  $T$ . These prerequisites are perfectly met the realization of the DF<sup>11</sup>. Beside, owing to the depairing of charge and heat currents in the hydrodynamics regimes, the DF is expected to reveal an enhancement of  $\kappa$  and the large-violated WF law in magnitude of hundreds of  $L/L_0$ , which are in good agreement with the observations. Therefore, our findings may provide firm experimental evidence for the potential existence of DF even in materials other than electron-hole plasma in graphene.

## **Conclusion**

So far, the main stream of the hydrodynamic study was to find the significant features, where either electron or phonon attributes primary scattering. However, all the transport regime – ballistic, hydrodynamic, and diffusive regimes – can coexist and coupled each other, so that it becomes more complicated and hard to observe purely quasiparticles hydrodynamic phenomena. With the ultrahigh purity of single crystals of  $\text{ZrTe}_5$ , we find the transport signature of the hydrodynamic-like behavior presumably result from the other types of quasiparticle excitations. Significantly violated the Lorenz ratio over the hundreds and non-trivial transport behavior in the vicinity of hydrodynamic regime, all the experimental observations indicate the DF induced by the charge-neutral plasma of quasi-relativistic fermions.

## **ACKNOWLEDGEMENT**

We gratefully thank Dr Benjamin Piot, the researcher scientist in Grenoble High Magnetic Field Laboratory (CNRS-LNCMI), for enlightening discussions.

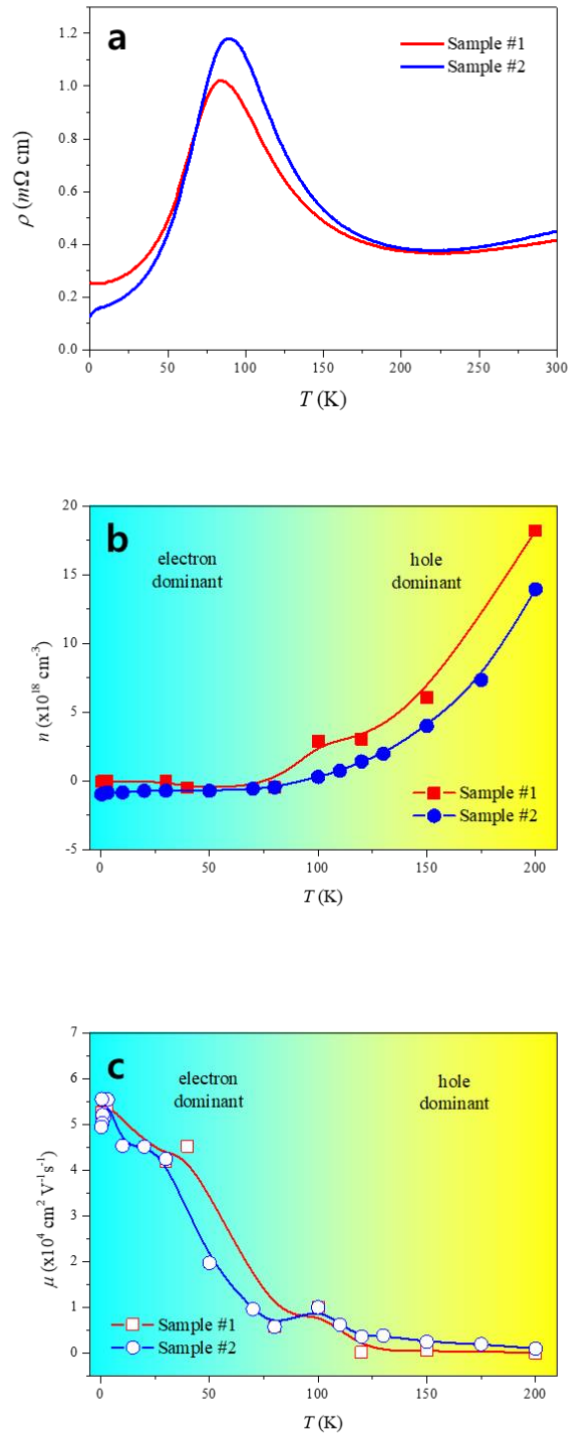


**Figure 1.** (Color Online) The temperature-dependent electrical resistivity  $\rho$  (a), the dominant carrier density  $n$  (b), and their mobility  $\mu$  (c) of ZrTe<sub>5</sub> single crystals. To extract the  $n$  and  $\mu$ , a two-band model was used for high  $T$  data (above 40 K), while the values in low  $T$  (below 40 K) were taken by the linear fit method from the Hall measurement.



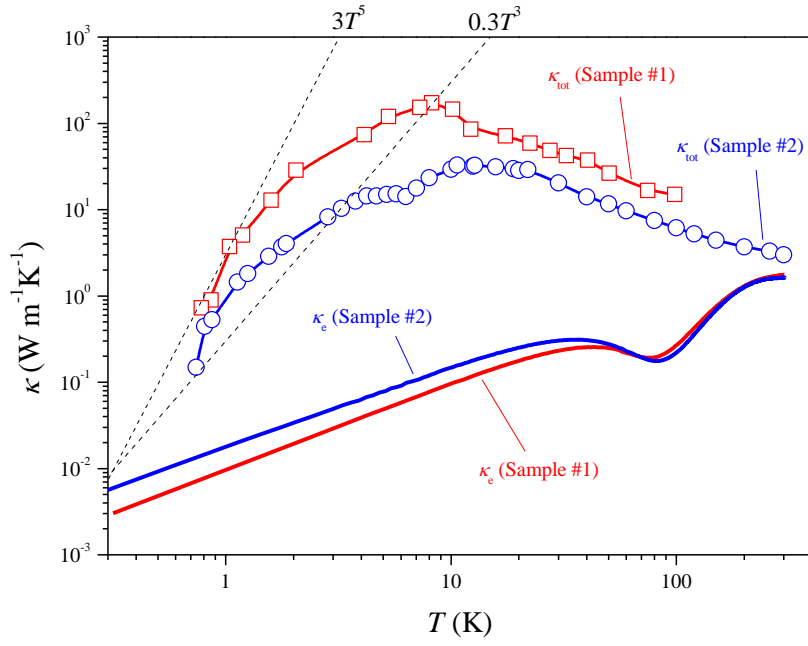


**Figure 2.** (Color Online) Thermal conductivity as a function of temperature in a log-log plot for two different  $\text{ZrTe}_5$  samples. The open squares (sample #1) and circles (sample #2) data represent total thermal conductivity  $\kappa_{tot}$ , and the solid lines denote charge carrier thermal conductivity  $\kappa_e$ , which is calculated by the Wiedemann-Franz law ( $\kappa_e = \frac{T}{\rho} L_0$ , where the Lorenz number  $L_0 = 2.44 \times 10^{-8} \text{ W}\Omega\text{K}^{-2}$ ). The two dashed lines proportional to  $T^3$  and  $T^5$  are added for comparison with  $\kappa_{tot}$  temperature evolution.

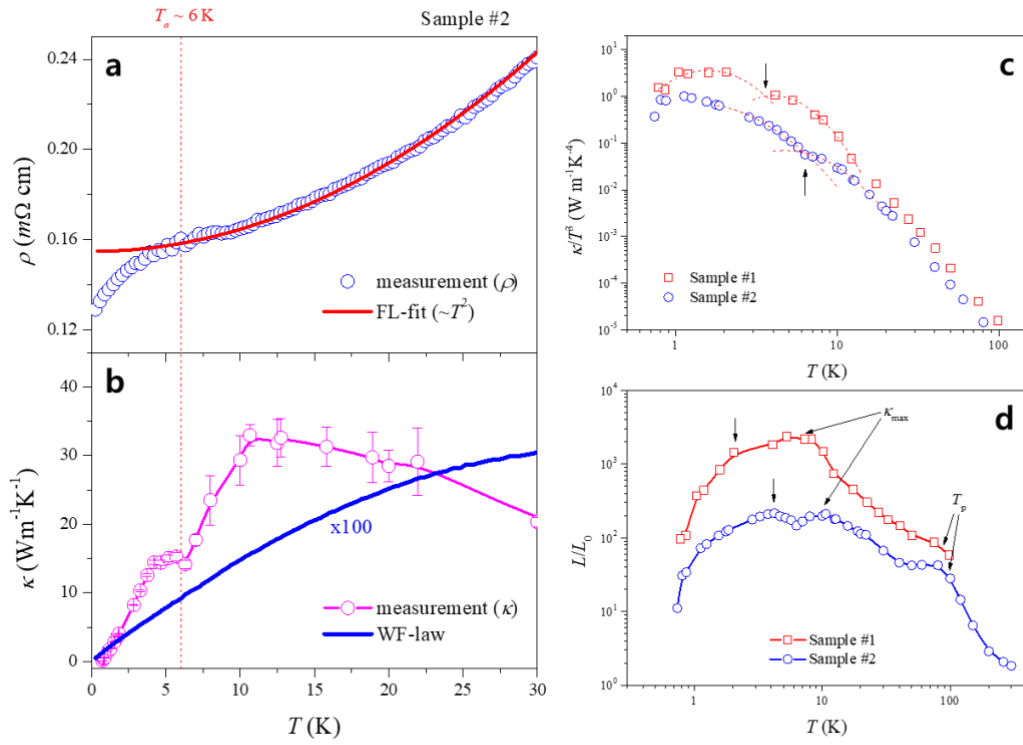


**Figure 3.** (Color Online) **(a, b)** The low-temperature electrical resistivity and the thermal conductivity for sample #2. The solid line (red) in **(a)** indicates a fit result of the usual Fermi-liquid behavior. The Wiedemann-Franz law curve in **(b)** is plotted with magnification of 100 for the better comparison. **(c)**  $\kappa/T^3$  and **(d)** Lorentz ratio ( $L/L_0$ ) of two samples as a function of temperature. All figures are plotted in a log-log scale. The vertical arrows in **(c)** and **(d)** indicate the kink and shoulder points, respectively. The dashed lines (red) in **(c)** are interpolated curves to show the kink-like anomaly.

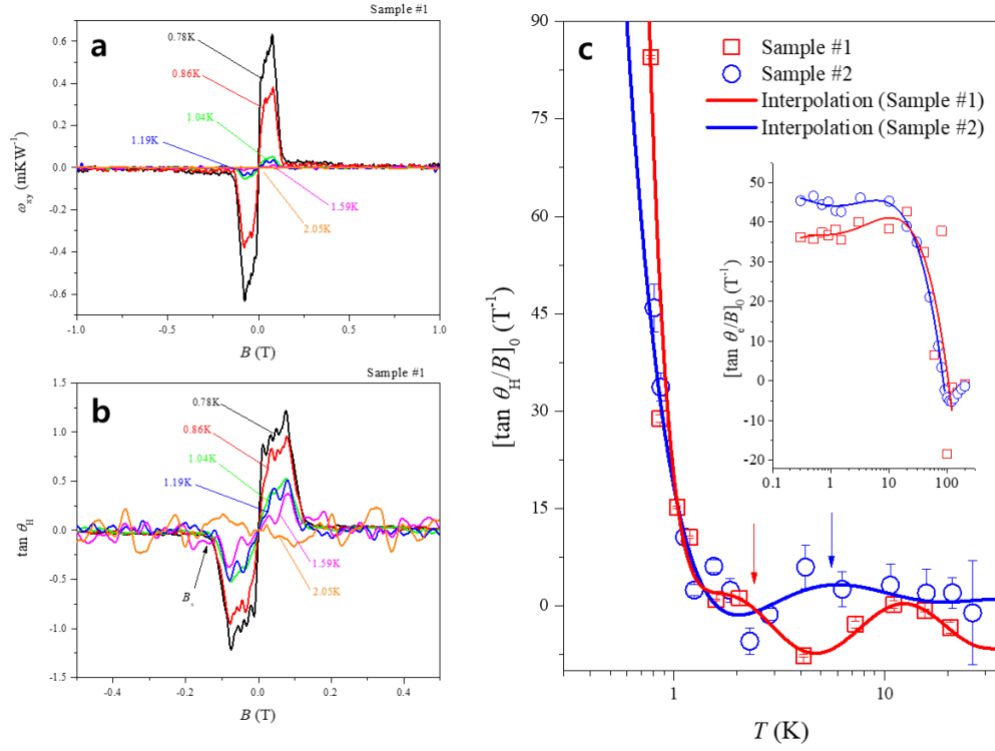


**Figure 4.** (Color Online) **(a)** The magnetic field dependence of thermal Hall resistivity  $\omega_{xy}$  at different temperatures (sample #1). **(b)** Tangential Hall angle ( $\tan \theta_H = \frac{\kappa_{xy}}{\kappa_{xx}}$ ) in a magnetic field range of -0.5 to 0.5 T with various temperatures (sample #1). **(c)** Temperature dependent slope of  $\tan \theta_H$  versus of  $B$  at a zero magnetic field limit for two samples. Only x-axis is presented with a log-scale. In general, this value is proportional to the quasiparticle mean-free-path. Inset of **(c)** exhibits an initial slope of an electronic Hall angle as same as thermal Hall angle. Each vertical arrows denote the local maxima.

## REFERENCES

1. S. R. Phillpot and A. J. H. McGaughey, *Materials Today* **8** (6), 18-20 (2005).
2. M. Kaviany, *Principles of Heat Transfer*. (Wiley, New York, 2002).
3. J. M. Ziman, *Electrons and Phonons: The Theory of Transport Phenomena in Solids*. (Oxford Univ. Press, 2001).
4. M. S. Dresselhaus, G. Chen, M. Y. Tang, R. G. Yang, H. Lee, D. Z. Wang, Z. F. Ren, J.-P. Fleurial and P. Gogna, *Adv. Mater.* **19**, 1043-1053 (2007).
5. C. C. Ackerman, B. Bertman, H. A. Fairbank and R. A. Guyer, *Phys. Rev. Lett.* **16**, 789-791 (1966).
6. W. J. De Haas and T. Biermasz, *Physica* **4**, 752-756 (1937).
7. S. Lee, D. Broido, K. Esfarjani and G. Chen, *Nat. Commun.* **6**, 6290 (2015).
8. Y. Machida, N. Matsumoto, T. Isono and K. Behnia, *Science* **367**, 309-312 (2020).
9. Y. Machida, A. Subedi, K. Akiba, A. Miyake, M. Tokunaga, Y. Akahama, K. Izawa and K. Behnia, *Sci. Adv.* **4**, eaat3374 (2018).
10. S. Huberman, R. A. Duncan, K. Chen, B. Song, V. Chiloian, Z. Ding, A. A. Maznev, G. Chen and K. A. Nelson, *Science* **364**, 375-379 (2019).
11. J. Crossno, J. K. Shi, K. Wang, X. Liu, A. Harzheim, A. Lucas, S. Sachdev, P. Kim, T. Taniguchi, K. Watanabe, T. A. Ohki and K. C. Fong, *Science* **351**, 1058-1061 (2016).
12. V. Martlli, J. L. Jimenez, M. Continentino, E. Baggio-Saitovitch and K. Behnia, *Phys. Rev. Lett.* **120**, 125901 (2018).
13. J. A. Sussmann and A. Thellung, *Proc. Phys. Soc.* **81**, 1122 (1963).
14. R. A. Guyer and J. A. Krumhansl, *Phys. Rev.* **148**, 778 (1966).
15. A. Cepellotti, G. Fugallo, L. Paulatto, M. Lazzeri, F. Mauri and N. Marzari, *Nat. Commun.* **6**, 6400 (2015).
16. X. Li and S. Lee, *Phys. Rev. B* **99**, 085202 (2019).
17. V. Martelli, J. L. Jimenez, M. Continentino, E. Baggio-Saitovitch and K. Behnia, *Phys. Rev. Lett.* **120**, 125901 (2018).
18. F. Tang, Y. Ren, P. Wang, R. Zhong, J. A. Schneeloch, S. A. Yang, K. Yang, P. A. Lee, G. D. Gu, Z. Qiao and L. Zhang, *Nature* **569**, 537 (2019).
19. H. Weng, X. Dai and Z. Fang, *Phys. Rev. X* **4**, 011002 (2014).
20. Q. Li, D. E. Kharzeev, C. Zhang, Y. Huang, I. Pletikoscic, A. V. Fedorov, R. D. Zhong, J. A. Schneeloch, G. D. Gu and T. Valla, *Nature Physics* **12** (6), 550+ (2016).
21. Z. Fan, Q.-F. Liang, Y. B. Chen, S.-H. Yao and J. Zhou, *Sci. Rep.* **7** (2017).
22. J. Mutch, W.-C. Chen, P. Went, T. Qian, I. Z. Wilson, A. Andreev, C.-C. Chen and J.-H. Chu, *Sci. Adv.* **5** (2019).
23. B. Xu, L. X. Zhao, P. Marsik, E. Sheveleva, F. Lyzwa, Y. M. Dai, G. F. Chen, X. G. Qiu and C. Bernhard, *Phys. Rev. Lett.* **121**, 187401 (2018).
24. W. Zhang, P. Wang, B. Skinner, R. Bi, V. Kozii, C.-W. Cho, R. Zhong, J. A. Schneeloch, D. Yu, G. D. Gu, L. Fu, X. Wu and L. Zhang, *Nat. Commun.* **11** (2020).
25. H. Chi, C. Zhang, G. D. Gu, D. E. Kharzeev, X. Dai and Q. Li, *New J. Phys.* **19**, 015005 (2017).
26. Y. Zhou, J. Wu, W. Ning, N. Li, Y. Du, X. Chen, R. Zhang, Z. Chi, X. Wang, X. Zhu, P. Lu, C. Ji, X. Wan, Z. Yang, J. Sun, W. Yang, M. Tian, Y. Zhang and H.-K. Mao, *Proc. Natl. Acad. Sci. USA* **113**, 2904 (2016).
27. C. Fu, T. Scaffidi, J. Weissman, Y. Sun, R. Saha, S. J. Watzman, A. K. Srivastava, G. Li, W. Schnelle, P. Werner, M. E. Kamminga, S. Sachdev, S. S. P. Parkin, S. A. Hartnoll, C. Felser and J. Gooth, *arXiv*, 1802.09468 (2018).
28. M. Hirschberger, J. W. Krizan, R. J. Cava and N. P. Ong, *Science* **348** (6230), 106-109 (2015).

**Supplementary Information for**  
**Observation of hydrodynamic-like behavior in 3D Dirac semimetal**  
**ZrTe<sub>5</sub>**

**Chang-woo Cho<sup>1,2</sup>, Peipei Wang<sup>1</sup>, Fangdong Tang<sup>1</sup>, Sungkyun Park<sup>2</sup>, Mingquan He<sup>3</sup>, Rolf Lortz<sup>4</sup>, Genda Gu<sup>5</sup>, and Liyuan Zhang<sup>1,+</sup>**

*<sup>1</sup>Department of Physics, Southern University of Science and Technology, 1088 Xueyuan Road, Nanshan District, Shenzhen, Guangdong 518055, China*

*<sup>2</sup>Department of Physics, Pusan National University, Busan 46241, South Korea*

*<sup>3</sup>Chongqing Key Laboratory of Soft Condensed Matter Physics and Smart Materials, College of Physics, Chongqing University, Chongqing 401331, China*

*<sup>4</sup>Department of Physics, The Hong Kong University of Science and Technology, Clear Water Bay, Kowloon, Hong Kong*

*<sup>5</sup>Condensed Matter Physics and Materials Science Department, Brookhaven National Laboratory, Upton, NY 11973, USA*

---

<sup>+</sup> corresponding author: zhangly@sustech.edu.cn

## 1. Thermal conductivity experimental set-up

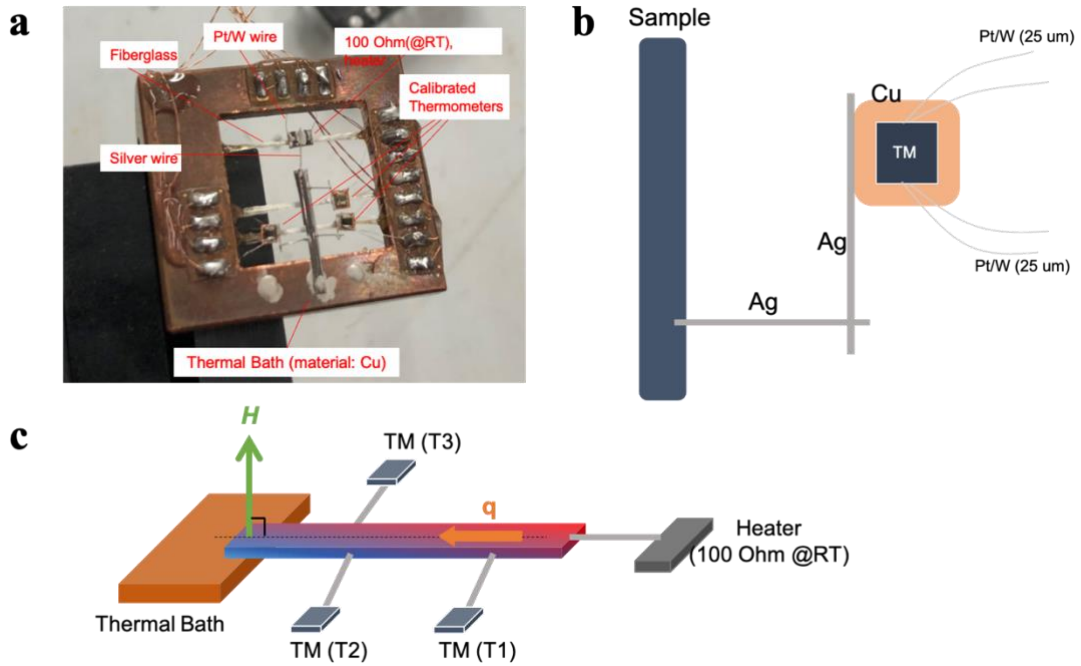


**Figure S3.** (a) The photo image of thermal conductivity setup used in this study. (b) To minimize the thermal leak from the resistive heater to thermal bath, we connected the sample to a resistive heater and thermometers through 100  $\mu\text{m}$  of thick Ag-wires, which is a good thermal conductor. While the connections for the electrical measurements are used by 25  $\mu\text{m}$  of thin Pt/W-wires, which is a good electrical conductor but a relatively bad thermal conductor. (c) Schematics of our thermal conductivity experiment.

## 2. Two different method for the thermal conductivity measurement: thermometers vs thermocouples

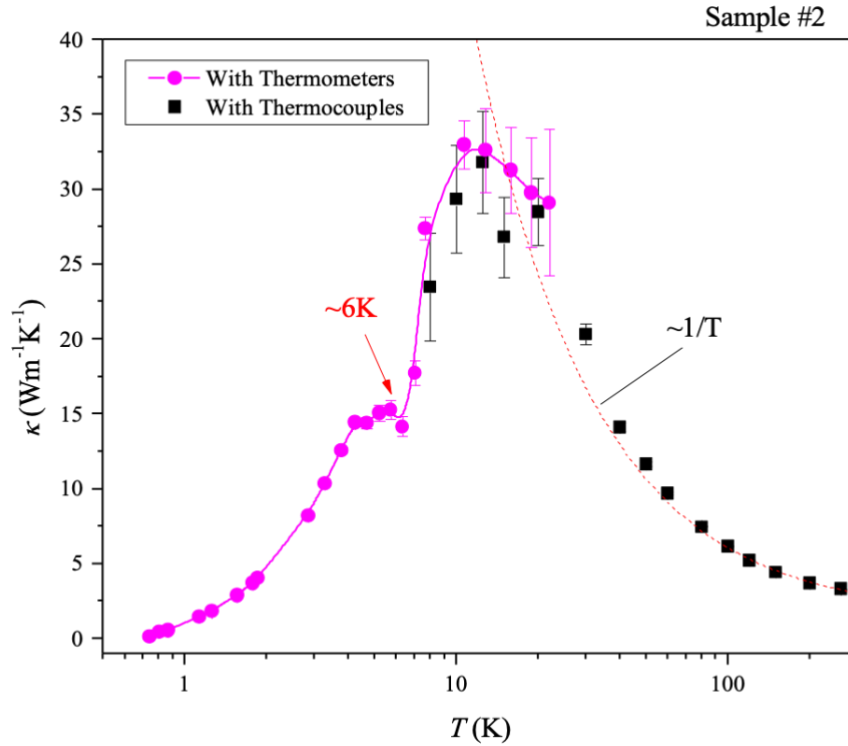


**Figure S2.** Thermal conductivity as a function of temperature for sample #2. Practically, thermometers are used for low temperatures calibration due to its semimetallic-like resistivity vs temperature behavior (magenta). On the other hand, thermocouples are more suitable at higher temperatures because of its metallic-like resistive curve (black). In our experiments, we observe the overlap temperature range of  $\sim 10$  to  $\sim 20$  K. The dotted line (red) denotes the  $1/T$  dependence curve.

### 3. Magnetic field dependence of electrical resistivity (sample #2)

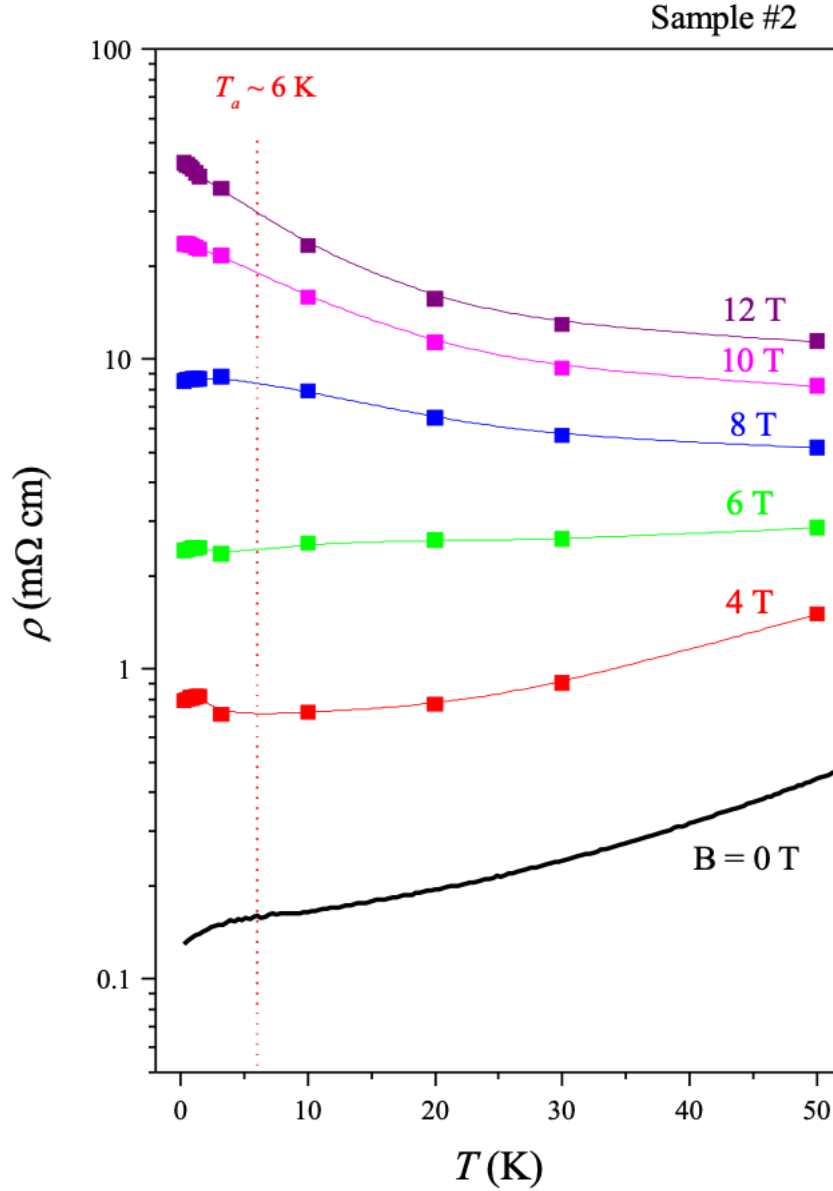


**Figure S3.** Temperature dependence of electrical resistivity at various applied magnetic fields. The data at 0 T is only measured, while others are extracted from the magneto-resistance (MR) measurements. An anomaly at  $T_a$  is seen at least until 8 T, which is exceeding to reported the critical field of pressured superconducting ZrTe<sub>5</sub>.